Supplementary Information (SI) for Physical Chemistry Chemical Physics.
This journal is © the Owner Societies 2026

Surface sites drive Fe enrichment at reactive olivine interfaces

Electronic Supporting Information

Ming Geng[*ab], Hannes Jónsson [b], Kunfeng Qiu[a] and Jun Deng[a]

a. School of Earth Sciences and Resources, China University of Geosciences, Beijing 100083, China.

b. Science Institute and Faculty of Physical Sciences, University of Iceland, VR-III, Reykjavík 107, Iceland.

Computation Methods

Density functional theory (DFT) calculations were carried out using the Vienna ab initio simulation package (VASP)**.** [1, 2] The exchange–correlation energy was described using the Perdew–Burke–Ernzerhof (PBE) functional within the generalized gradient approximation (GGA). A plane-wave kinetic energy cutoff of 700 eV was employed throughout. The interaction between valence electrons and ionic cores was treated using the projector augmented wave (PAW) method. Monkhorst–Pack k-point meshes of 8 × 8 × 8 and 8 × 8 × 1 were used for bulk crystal and slab calculations, respectively. The relatively high cutoff energy and dense k-point sampling were adopted to obtain stable relative energies among Fe/Mg configurations. Because the present study compares small energy differences associated with Fe occupation at different crystallographic and surface sites, a conservative numerical setup was used to reduce convergence-related uncertainty (Fig. S2). The k-point sampling follows our previous surface calculations on Mg-endmember forsterite[3], while the cutoff energy was increased for the present Fe-bearing systems. To minimize the effect of the periodic boundary conditions, a 30 Å-thick vacuum space is added on top of the surface slab models. Structural optimizations were performed until the residual force on each atom was less than 0.01 eV $Å^{-1}$.

Because Fe-bearing silicates may exhibit different spin states, all calculations were performed within a spin-polarized framework. In octahedral coordination, the Fe 3d orbitals are split into t^{2g} and e^{g} manifolds. For Fe^{2+}, both high-spin and low-spin states were considered. The high-spin state corresponds to S = 2 (2S + 1 = 5), whereas the low-spin state corresponds to S = 0 (2S + 1 = 1). Since spin transitions are known to occur in many Fe-bearing mantle minerals,

spin polarization is required for a proper description of their electronic structure[4, 5].

To further assess the robustness of the bulk energetic ordering, additional calculations were carried out using both the DFT+U approach and the strongly constrained and appropriately normed (SCAN) meta-GGA functional[6]. In the DFT+U calculations, the on-site Coulomb parameters for Fe were taken as U = 4.5 eV and J = 0.9 eV, following previous studies[7-9]. Because SCAN calculations may occasionally encounter convergence difficulties during structural optimization, the PBE-optimized structures were used as the initial configurations for subsequent SCAN and PBE+U calculations.

Surface models were constructed using slab geometries. Because the distribution of Fe atoms in the slab models is not always symmetric, dipole corrections were included in the slab calculations. Bulk and surface models with different Fe/Mg arrangements were examined to evaluate the relative stability of Fe occupation at distinct crystallographic and interfacial sites.

Thermodynamic analysis

the Gibbs free energy was evaluated as

$$G(T) = E_{DFT} + F^{vib}(T) - TS^{conf} + pV \quad (1)$$

where E_{DFT} is the ground-state total energy obtained from DFT, $F^{vib}(T)$ is the vibrational free-energy contribution, and Sconf is the configurational (mixing) entropy. The unit-cell volume is 299.12 A˚3. Experimental data indicate that the volume variation below 15 GPa is very small, so the pV term is expected to be comparable to the intrinsic uncertainty of the DFT calculations. In addition, for comparisons between structures of the same composition, the volume differences are extremely small. Therefore, the pV term was neglected in the evaluation of relative Gibbs free energies, and the free-energy difference between two configurations was written as

$$\Delta G(T) = \Delta E + \Delta F^{vib}(T) - T\Delta S^{conf} \quad (2)$$

The configurational entropy was evaluated explicitly to account for different distributions of Fe atoms among crystallographic sites,

$$S^{conf} = -k_B \sum_j \left(m_j \sum_i X_{ij} \ln X_{ij} \right) \quad (3)$$

where m_j is the total number of atoms occupying the j-th crystallographic site, and X_{ij} is the mole fraction of species i at site j.

The vibrational free-energy contribution was calculated from the phonon frequencies as

$$F^{vib}(T) = \frac{1}{2}\sum_{qj} h\omega_{qj} + k_B T \sum_{qj} ln\left[1 - e^{\left(-h\omega_{qj}\right)/k_B T}\right] \quad (4)$$

where q is the wave vector, j is the phonon branch index, and ω_{qj} is the phonon frequency of mode (q,j). Phonon calculations were carried out using density functional perturbation theory (DFPT) as implemented in the VASP/Phonopy package[10].

Bader charge and Fe valence assignment

Fe was introduced by isovalent substitution of Mg at the metal sites of the olivine structure, corresponding formally to Fe^{2+} substitution for Mg^{2+}. To examine whether the optimized structures preserve a consistent Fe chemical state, Bader charge analyses were performed for the relaxed bulk and slab configurations. The calculated Fe Bader charges are broadly consistent among the examined configurations, while surface Fe sites show some variation due to undercoordination and charge redistribution at the interface. Since Bader charges are not formal oxidation states and are not expected to be integer values, they are used here as a relative measure of charge distribution. The results are consistent with Fe remaining in a divalent-like state across the examined configurations. Bader charge and Bader volume analyses provide complementary information on the local charge distribution and spatial accommodation of Fe and Mg at surface and interior sites. These analyses support the structural interpretation that undercoordinated surface sites provide greater local relaxation freedom for Fe. However, they are not intended to replace a full orbital-resolved electronic-structure analysis, which will be useful in future work.

Preliminary adsorption-energy calculations

To provide an initial assessment of whether Fe-rich and Mg-rich surface sites interact differently with fluid molecules, preliminary adsorption-energy calculations were performed for selected molecules on representative olivine surface sites. The adsorption energy was calculated as

$E_{ads} = E_{slab} + molecule - E_{slab} - E_{molecule}$With this definition, more negative values indicate stronger adsorption. These calculations are intended only as a first-order comparison of molecule–surface interactions and are not used to infer complete reaction mechanisms or reaction barriers. The results are shown in Fig. S6.

Table S1: Experimental and Calculated Values for Cell Parameters of Bulk Forsterite (in Å)

Lattice Constant	Experiment			This work		
	Forsterite	Fo50	Fayalite	Fo75	Fo50	Fo25
a	4.76	4.81	4.82	4.83	4.88	4.88
b	10.20	10.38	10.49	10.50	10.51	10.51
c	5.98	6.06	6.10	6.14	6.16	6.16

Table S2:Bader volumes (Å³) for the M2-terminated slab with 2 Fe atoms

Layer	Top Fe	Top Mg	Mid Fe	Mid Mg
Top	M1: 159.6	M1: 106.8	M1: — ; M2: —	M1: 4.9 ; M2: 5.3
Sub	—	M2: 92.8	M1: 10.8	M1: 4.9 ; M2: 5.2
Sub-II	—	M2: 93.0	M1: 10.8	M1: 4.9 ; M2: 5.2
Mid	—	M2: 94.8	M2: 10.9	M1: 4.9 ; M2: 5.4
Mid-II	—	M2: 93.4	M2: 11.0	M1: 4.9 ; M2: 5.2

Table S3:Bader volumes (Å³) for the M1-terminated slab with 2 Fe atoms

Layer	Top Fe	Top Mg	Mid Fe	Mid Mg
Top	M1: 69.0	M1: 9.1	—	M1: 4.9 ; M2: 5.3
Sub	—	M1: 8.7	M2: 11.2	M1: 4.9 ; M2: 5.4
Sub-II	—	M1: 8.8	M2: 11.2	M1: 4.9 ; M2: 5.4
Mid	—	M1: 9.3	M1: 10.6	M1: 5.0 ; M2: 5.4
Mid-II	—	M1: 9.1	M1: 10.3	M1: 5.0 ; M2: 5.4

Table S4: Bader charges (e) for the M2-terminated slab with 2 Fe atoms

Layer	Top Fe	Top Mg	Mid Fe	Mid Mg
Top	M1: 1.22	M1: 1.67	M1: — ; M2: —	M1: 1.68 ; M2: 1.70
Sub	—	M2: 1.67	M1: 1.32	M1: 1.68 ; M2: 1.70
Sub-II	—	M2: 1.66	M1: 1.32	M1: 1.68 ; M2: 1.70
Mid	—	M2: 1.66	M2: 1.38	M1: 1.68 ; M2: 1.70
Mid-II	—	M2: 1.64	M2: 1.38	M1: 1.68 ; M2: 1.70

Table S5: Bader charges (e) for the M1-terminated slab with 2 Fe atoms

Layer	Top Fe	Top Mg	Mid Fe	Mid Mg
Top	M1: 1.15	M1: 1.65	—	M1: 1.68 ; M2: 1.70
Sub	—	M1: 1.65	M2: 1.35	M1: 1.68 ; M2: 1.70
Sub-II	—	M1: 1.65	M2: 1.35	M1: 1.68 ; M2: 1.70
Mid	—	M1: 1.65	M1: 1.33	M1: 1.68 ; M2: 1.70
Mid-II	—	M1: 1.65	M1: 1.31	M1: 1.68 ; M2: 1.70

Table S6:Bader volumes (Å³) for the M2-terminated slab with 4 Fe atoms

Layer	Top Fe	Top Mg	Mid Fe	Mid Mg
TwoTop	M2: 162.3	—	—	M1: 4.9 ; M2: 5.3
Top-Sub	M2: 90.1	110.3	M1: 11.1	M1: 4.9 ; M2: 5.3
Top-Sub-II	M2: 125.7	104.6	M1: 10.9	M1: 4.9 ; M2: 5.3
Top-Mid	M2: 157.2	108.4	M2: 10.9	M1: 4.9 ; M2: 5.2
Top-Mid-II	M2: 157.7	106.3	M2: 10.8	M1: 4.9 ; M2: 5.3
Top-Mid-III	M2: 158.1	102.8	M1: 10.9	M1: 4.9 ; M2: 5.2
Sub	—	88.4	M1: 10.7	M1: 4.9 ; M2: 5.2
Sub-II	—	89.2	M1: 10.8	M1: 4.9 ; M2: 5.3
Sub-III	—	87.9	M1: 10.8	M1: 4.9 ; M2: 5.3
Mid	—	91.6	M2: 11.0	M1: 4.9 ; M2: 5.2

Table S7: Bader charges (e) for the M2-terminated slab with 4 Fe atoms

Layer	Top Fe	Top Mg	Mid Fe	Mid Mg
TwoTop	M2: 1.23	—	—	M1: 1.68 ; M2: 1.70
Top-Sub	M2: 1.14	1.67	M1: 1.31	M1: 1.68 ; M2: 1.70
Top-Sub-II	M2: 1.17	1.67	M1: 1.33	M1: 1.68 ; M2: 1.70
Top-Mid	M2: 1.22	1.67	M2: 1.39	M1: 1.68 ; M2: 1.70
Top-Mid-II	M2: 1.21	1.67	M2: 1.38	M1: 1.68 ; M2: 1.70
Top-Mid-III	M2: 1.22	1.67	M1: 1.39	M1: 1.68 ; M2: 1.70
Sub	—	1.67	M1: 1.32	M1: 1.68 ; M2: 1.70
Sub-II	—	1.67	M1: 1.32	M1: 1.68 ; M2: 1.70
Sub-III	—	1.67	M1: 1.32	M1: 1.68 ; M2: 1.70
Mid	—	1.67	M2: 1.38	M1: 1.68 ; M2: 1.70

Figure S1: Structure of olivine crystal (Fo50 as an example) M1 and M2 site are two types of metal cation site, both of these sites with the oxygen around formed two types of octahedra. Silicon and oxygen atoms formed tetrahedra.

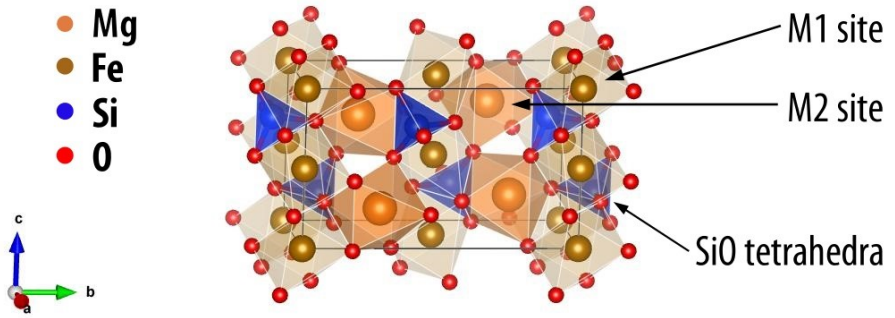

Figure S2: Convergence test for ENCUT. Energy Diff shows energy differences associated with Fe occupation at different crystallographic sites M1 and M2.

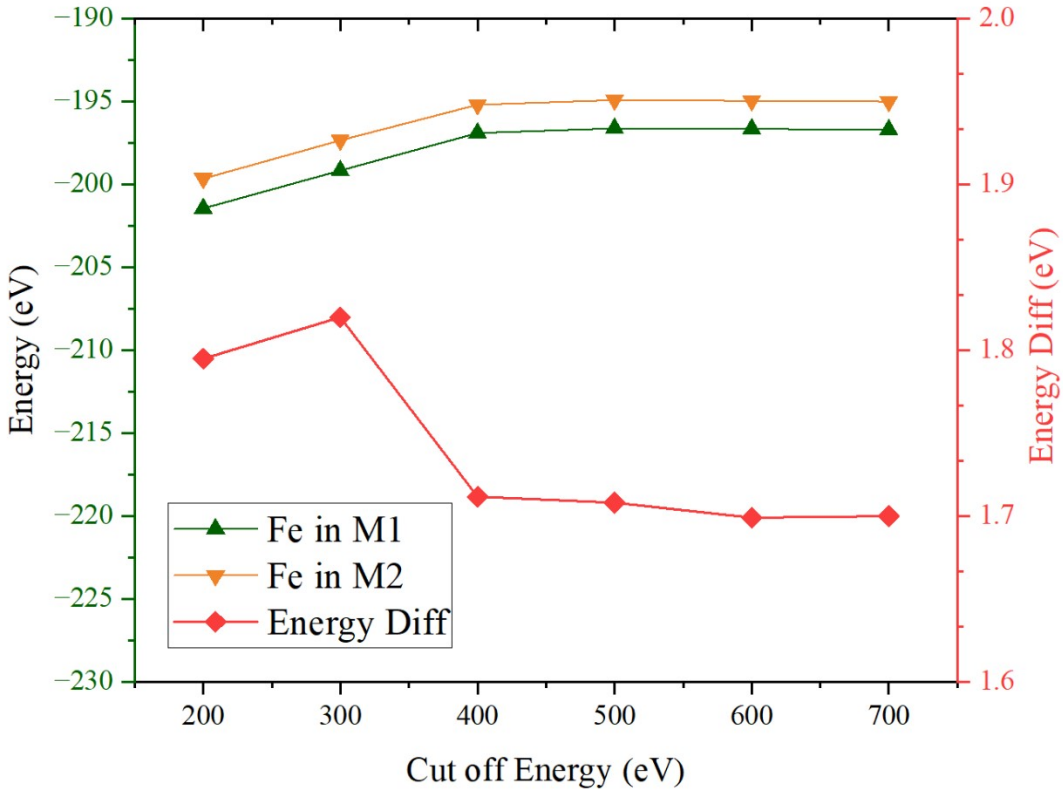

Figure S3: Structures of the $(Mg_xFe_{2-x})SiO_4$ with different Fe distribution in iron rich (Fo25) and iron poor (Fo75). The structure is named by the metal atom number in M1 sites. k_D is the distribution coefficient. The k_D value shift with the structure chemical composition.

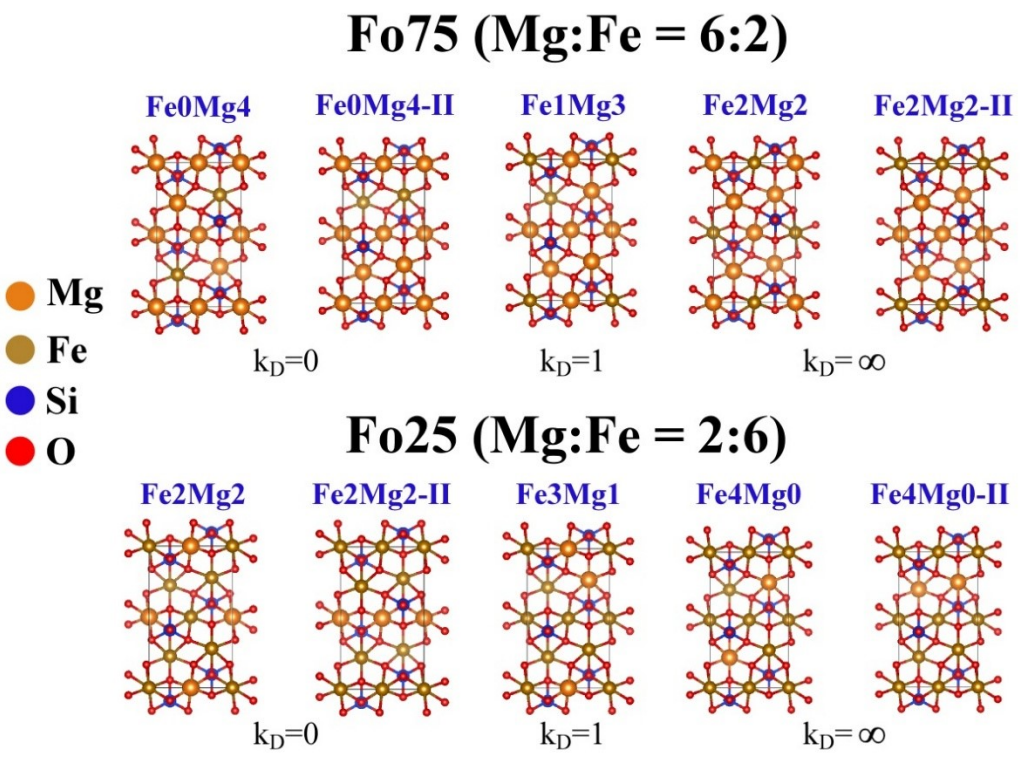

Figure S4: Atom displacements between origin cleaved slab and relaxed slabs grouped by the different surface termination and Fe concentration. The displacement $d = \frac{\Delta Z_{i,j}^{origin} - \Delta Z_{i,j}^{relaxed}}{\Delta Z_0}$, $\Delta Z_{i,j}^{origin}$ **is the distance between atoms i and j in unrelaxed slab,** $\Delta Z_{i,j}^{relaxed}$ **is the distance between atoms i and j in relaxed slab,** ΔZ_0 **is the length of thickness of the surface slab. In all relaxed slab models, the SiO_4 tetrahedra remain intact and the characteristic olivine M-site framework is preserved. Structural relaxation is mainly localized near the exposed surface region, whereas the inner slab remains bulk-like.**

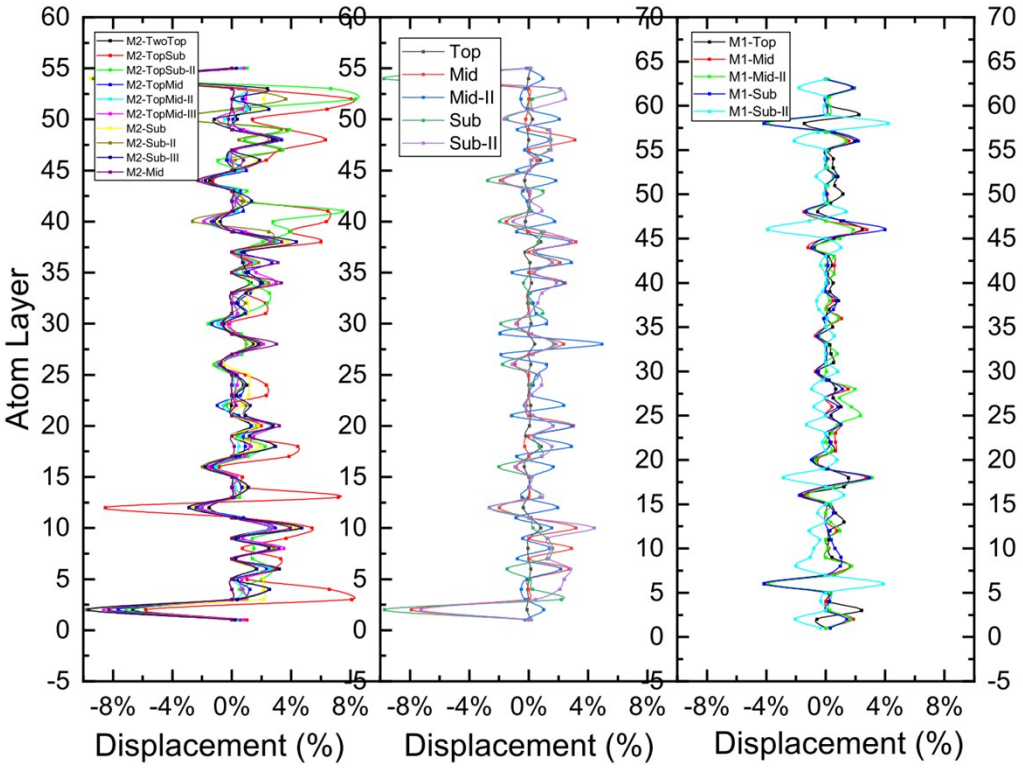

Figure S5: Side Views of structures of the slabs with different Fe distribution and different terminations. M2 termination and M1 termination mean the slab have M2 or M1 site exposed on the surface respectively. The naming is based on the Fe atom location of the slab. Top means on the surface, Sub means under the surface, and Mid means inside the interior of the slab.

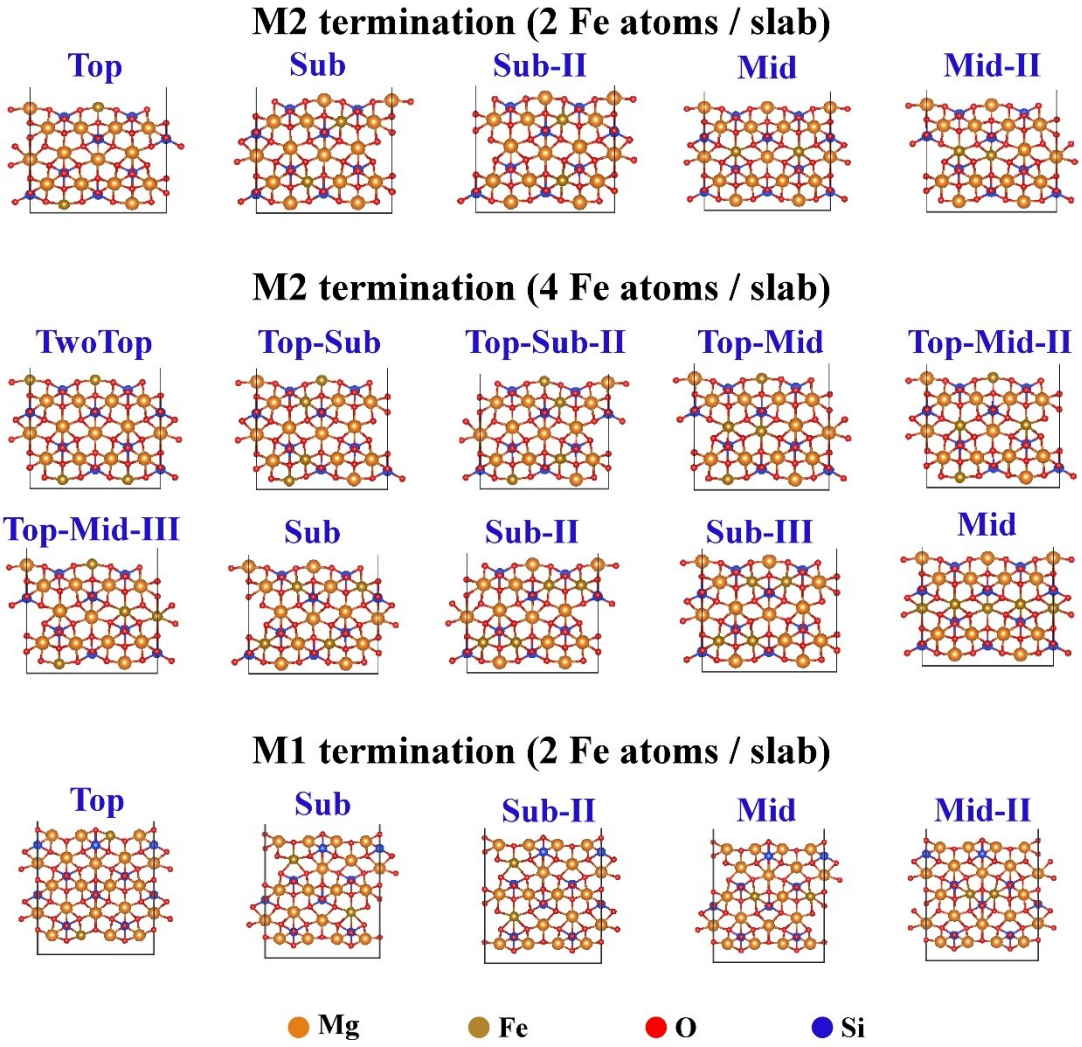

Figure S6: Preliminary adsorption-energy calculations of selected molecules on Mg-rich and Fe-rich olivine surface sites.

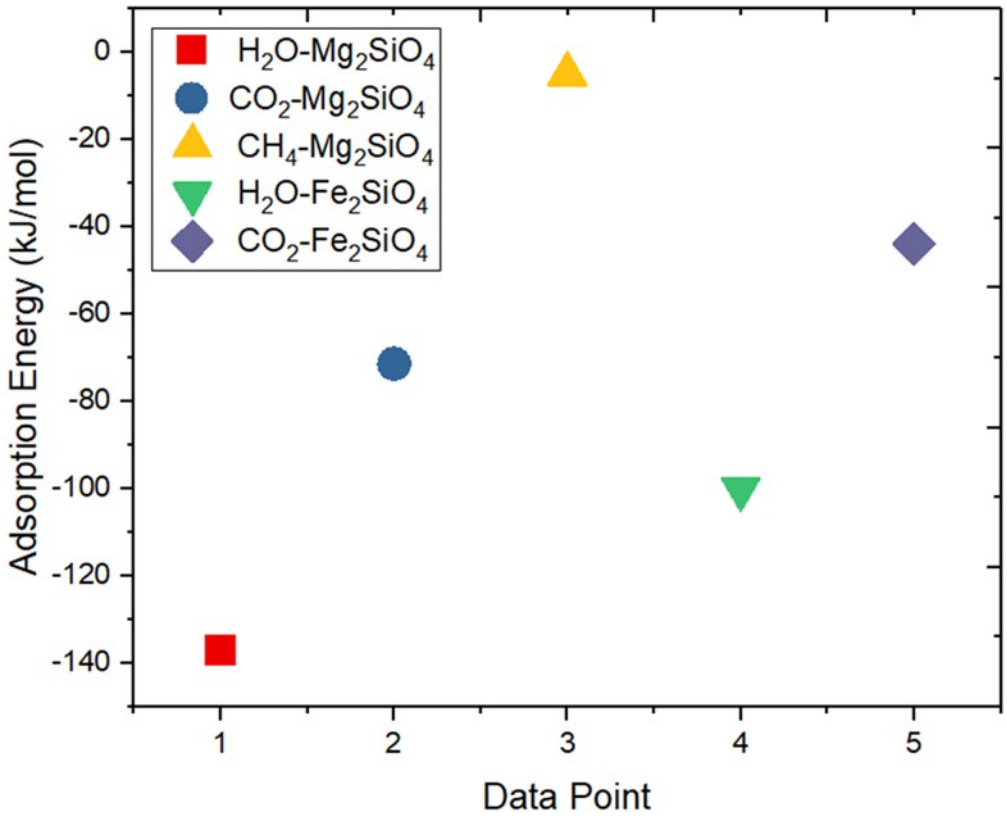

Reference

1. G. Kresse and J. Furthm\"uller, *Physical Review B*, 1996, **54**, 11169–11186.
2. G. Kresse and D. Joubert, *Physical Review B*, 1999, **59**, 1758–1775.
3. M. Geng and H. Jónsson, *The Journal of Physical Chemistry C*, 2019, **123**, 464–472.
4. T. Tsuchiya, R. M. Wentzcovitch, C. R. S. da Silva and S. de Gironcoli, *Physical Review Letters*, 2006, **96**, 198501.
5. E. Holmström and L. Stixrude, *Physical Review Letters*, 2015, **114**, 117202.
6. J. Sun, R. C. Remsing, Y. Zhang, Z. Sun, A. Ruzsinszky, H. Peng, Z. Yang, A. Paul, U. Waghmare, X. Wu, M. L. Klein and J. P. Perdew, *Nature chemistry*, 2016, **8**, 831–836.
7. L. Xiao, X. Li and X. Yang, *The European Physical Journal B*, 2018, **91**, 85.
8. X. Jiang and G. Y. Guo, *Journal of Magnetism and Magnetic Materials*, 2004, **282**, 287–290.
9. C.-Y. Zhang, X.-B. Wang, X.-F. Zhao, X.-R. Chen, Y. Yu and X.-F. Tian, *Chinese Physics B*, 2017, **26**, 126103.
10. A. Togo and I. Tanaka, *Scripta Materialia*, 2015, **108**, 1–5.